Journal of Nanobiotechnology

RESEARCH

Open Access

Ion osmolarity-driven sequential concentration-enrichment for the scale-up isolation of extracellular vesicles

Lizhi Wang[1], Junhao Xia[1], Xin Guan[1], Yang Song[1], Mengru Zhu[1], Fengya Wang[1], Baofeng Zhao[2], Lukuan Liu[1*] and Jing Liu[1*]

Abstract

Extracellular vesicles (EVs) carry a variety of bioactive molecules and are becoming a promising alternative to cell therapy. Scale-up EV isolation is necessary for their functional studies and biological applications, while the traditional methods are challenged by low throughput, low yield, and potential damage. Herein, we developed an ion osmolarity-driven sequential concentration-enrichment strategy (IOSCE) for the EV isolation. IOSCE is composed of a novel superabsorbent polymers (SAPs) for EV concentration and a charged polymer for EV enrichment. Based on the driving force of ionic osmotic pressure, IOSCE can isolate EVs on a large scale from cell culture medium. The saturated water absorption capacity of IOSCE is 13.62 times higher than that of commercial SAPs. Compared with the ultracentrifugation method, IOSCE exhibited a 2.64 times higher yield (6.33×10^8 particles/mL). Moreover, the mesenchymal stem cell-derived EVs isolated using IOSCE demonstrate strong biological activity and can reduce neuroinflammation by affecting RNA metabolism and translation processes. IOSCE provides a cost-effective, high-throughput, and low-damage method for the scale up EV isolation, which is promising for disease diagnosis and treatment.

Keywords Stem cell, Extracellular vesicles, Isolation, Neuroinflammation, Proteome

*Correspondence:
Lukuan Liu
lukuanliu@163.com
Jing Liu
liujing@dmu.edu.cn
Full list of author information is available at the end of the article

Graphical Abstract

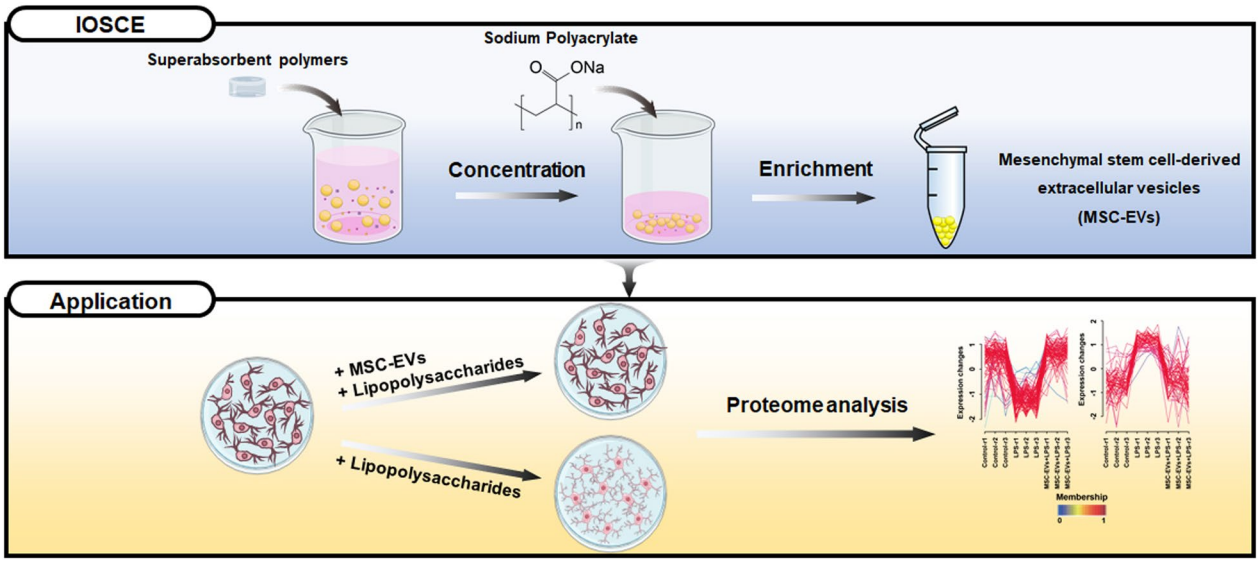

Introduction

Extracellular vesicles (EVs) are small phospholipid particles secreted by most cells, ranging in diameter from 30 to 1000 nm [1]. These vesicles play important roles in cellular regulation and material exchange, as they actively transport proteins, nucleic acids, and lipids [2–4]. These features make EVs not only minimally invasive biomarkers for various diseases [5–8] but also potential alternative to cell therapy. For example, mesenchymal stem cell-derived EVs (MSC-EVs) are used to treat neurodegenerative diseases, due to their abundance of anti-inflammatory and neuro-modulatory factors [9–14].

The clinical application of EVs faces significant challenges in achieving large-scale production while maintaining their biological activities. Ongoing clinical trials often require over 10^8 EVs per dose, necessitating the collection of substantial cell culture medium (CCM) over several months [15]. Furthermore, conventional isolation techniques struggle to achieve large-scale enrichment of biologically active EVs. For example, ultracentrifugation (UC) is considered the gold standard for EV isolation, but it is often limited by instrument capacity and the shear forces that can damage EV membranes [16–18]. Ultrafiltration (UF) and polymer precipitation, which have the potential for scale-up enrichment, suffer from membrane clogging and protein contamination, respectively, leading to reduced enrichment efficiency and purity [19].

The strategy of using superabsorbent polymers (SAPs) to concentrate CCM to reduce the initial sample volume has opened a new way to prepare EVs on a large scale [20]. However, due to the limitation of monomer types in the formula, the current commercial SAPs have a limited saturated water absorption capacity (4.5 mL/g), which restricts their concentration ability. In addition, the employment of size exclusion chromatography (SEC) for isolating EVs from concentrated samples entails the laborious collection of over 30 fractions to select samples of the highest purity. This approach is hindered by low efficiency and universality, posing a barrier to the efficient and large-scale isolation of EVs. Consequently, the development of more efficacious and universal concentration and enrichment strategies holds importance for advancing the large-scale production of EVs.

In this study, we developed an ion osmolarity-driven sequential concentration-enrichment strategy (IOSCE) for scale-up EV isolation, encompassing two main steps: concentration and enrichment. During the EV concentration process, we formulated a novel composition of SAPs and investigated the effects of crosslinking degree, salt concentration, and pH on the concentration capability, which lead to a saturated water absorption capacity 13.62 times greater than that of widely-used commercial SAPs. In the EV enrichment stage, charged polymer with scalable potential was used to neutralize the vesicle charge to enhance the specificity, considering the negatively charged nature of EV surfaces. Finally, we evaluated the biological activity of MSC-EVs obtained using IOSCE and found that MSC-EVs could reduce neuroinflammation by

affecting RNA metabolism and transcription, demonstrating their potential in clinical therapy.

Materials and methods

Materials

Sodium polyacrylate (SP), N-isopropylacrylamide, N,N′-methylene-bisacrylamide, Iodoacetamide, DL-Dithiothreitol, Ammonium bicarbonate and urea were obtained from Sigma. The BV2 mouse microglial cell line was purchased from the Shanghai Zhong Qiao Xin Zhou Biotechnology Co., Ltd. Umbilical cord MSCs used in this study was in accordance with principles of the Declaration of Helsinki and was approved by the Ethics Committee of the First Affiliated Hospital of the Dalian Medical University (registration number: PJ-KS-KY-2023-97). Other materials and the cell culture protocol are given in the Supporting Information (SI), Text S1 and S2.

Preparation and evaluation of the SAPs

A series of SAPs with varying degrees of cross-linking were synthesized as follows: 0.72 mL of acrylic acid were added to 4 mL of deionised water, followed by the addition of 0.26 g of sodium hydroxide to adjust the solution's neutralisation to 65%. Next, 0.485 g of N-isopropylacrylamide were dissolved with full stirring at 40 °C. After that, 0.006 g of potassium persulfate and varying proportions of cross-linking agent were added. The solution was then stirred at 600 rpm with a temperature of 40 °C. After complete dissolution, the temperature was subsequently increased to 60 °C with a reduction in stirring speed to enhance polymer chain formation and cross-linking. As the reaction proceeded, the viscosity of the mixture increased. The resulting gel-like substance was then subjected to thermal curing at 75 °C for 5 h. Following this, the polymer was dried at 60 °C for 24 h to remove any residual moisture, yielding the final SAPs (Figure S1). The evaluation protocol of SAPs is given in the SI, Text S3.

Molecular dynamics simulation

A molecular dynamics simulation was conducted by the GROMACS 2018.8 and the OPLS-AA force field, aimed at elucidating the chemical mechanism underlying water absorption in SAPs [21–27]. Detailed simulation parameters are provided in the SI, Text S4.

MSC-EVs isolation by the IOSCE

The CCM of MSCs was centrifuged at 200 g and 2000 g for 10 and 20 min at 4 °C, respectively. The supernatant was filtered by 0.22 μm cellulose acetate filter. Then the filtered liquid was concentrated by 10 mg/mL of SAPs. The concentrated medium was mixed with 4% SP solution at a ratio of 2:1, and incubated overnight at 4 °C, followed by centrifuging at 10,000 g for 1 h at 4 °C. The precipitate was then resuspended, and washed using PBS and $CaCl_2$ on a 100 kDa ultrafiltration membrane. The residue on the membrane was resuspended, yielding the final MSC-EVs. MSC-EVs isolation by UC and polyethylene glycol-based precipitation (PEG) are given in the SI, Text S5 and S6. For the detailed characterization of MSC-EVs, including nanoparticle tracking analysis (NTA), transmission electron microscopy (TEM), protein abundance and western blot (WB) analysis, please refer to the SI, Text S7, S8 and S9. For further details regarding scaled-up isolation of MSC-EVs by the IOSCE and the safety and biocompatibility assessments of MSC-EVs, please refer to the SI, Text S10 and S11.

Cell models of inflammatory response

BV2 cells were seeded in six-well plates. The control group received no treatment. In the prevention group, MSC-EVs (30 μg/mL) were added and incubated for 24 h, followed by LPS (0.5 μg/mL) stimulation for 24 h. The LPS group was stimulated with LPS (0.5 μg/mL) for 24 h. In the MSC-EVs group, MSC-EVs (30 μg/mL) was added and incubated for 24 h. After treatment, the cells and CCM of each group were collected for subsequent detection. The protocols to measure the MSC-EVs internalization, and the levels of IL-6, IL-1β and iNOS in the CCM of each group are given in the SI, Text S12 and S13.

Proteomics and bioinformatics analysis

Protein peptides were prepared using the filter-assisted sample pretreatment method for liquid chromatography-mass spectrometry/mass spectrometry (LC–MS/MS) analysis. The peptides were analysed on a SCIEX M5 MicroLC microlitre liquid chromatography coupled with a Triple-TOF 5600+mass spectrometer. The mass spectrum data for spectral library construction was retrieved by ProteinPilot software (v.5.0.2) with built-in Paragon algorithm. The detailed proteomic sample preparation, LC–MS/MS analysis, Data retrieval and quantitative analysis and bioinformatics analysis are provided in the SI, Text S14, S15, S16 and S17.

Results

Preparation and concentration performance of SAPs with ionic network

Volume reduction of CCM is necessary for the large-scale isolation of EVs. SAPs can concentrate CCM by ionic osmotic pressure-driven water absorption [20]. Water absorption efficiency of SAPs is influenced by the size of water channels formed by ion networks, which in turn is affected by salt and pH. In this study, SAPs with gradient crosslinking degrees and two monomers were prepared to optimize water absorption (Scheme 1, Table S1).

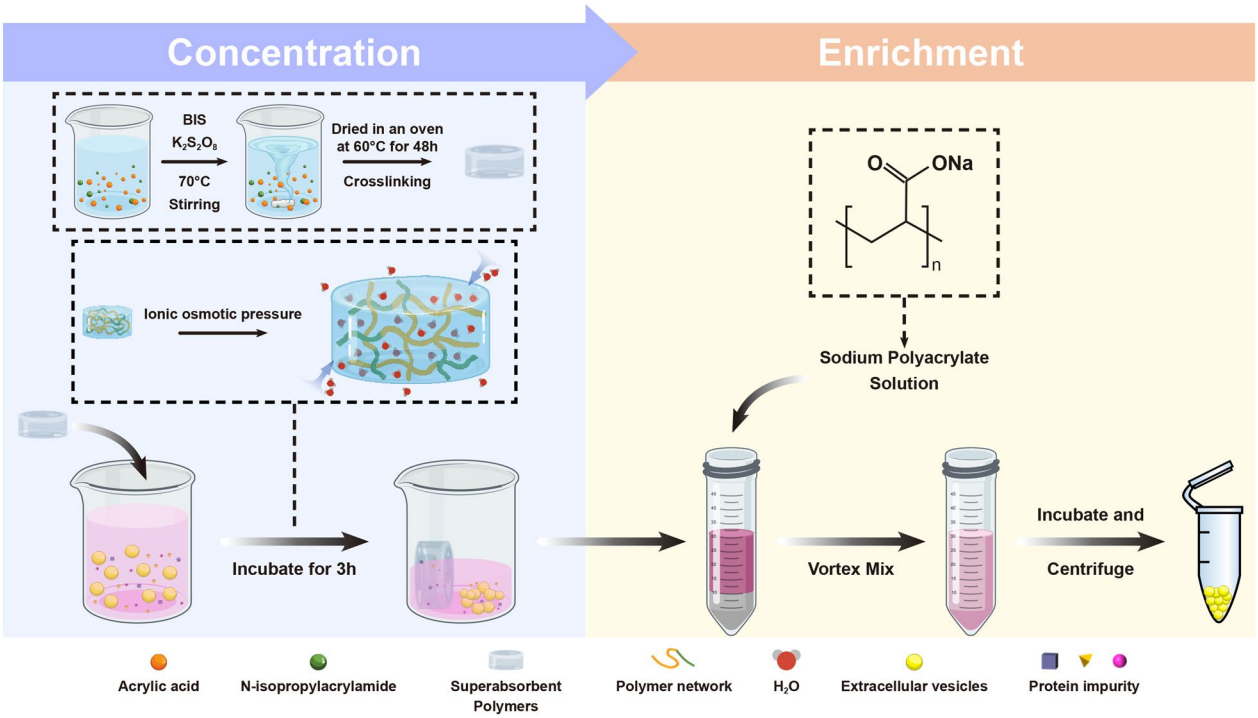

Scheme 1 Schematic for an ion osmolarity-driven sequential concentration-enrichment strategy (IOSCE)

The SAPs were categorized into low (SAP-0.25, SAP-0.5, and SAP-0.75), medium (SAP-1, SAP-2, and SAP-5), and high (SAP-10, SAP-15, and SAP-20) crosslinked groups based on their different crosslinking degrees. The adsorption behavior of SAPs was investigated by assessing their water volume reduction properties. The water volume decreased with increasing incubation time and reached a minimum after 180 min for different crosslinking degrees (Fig. 1A). For example, using 10 mg/mL of SAP-0.75, the average water absorption rate was 34.07 μL/min in the first 180 min, and between 180 and 420 min, it slowed to 6.53 μL/min reduced to 38.67% under these conditions. The saturation water absorption capacity of SAP-0.75 was 13.62 times that of the commercial SAPs [20]. As shown in Fig. 1B, the water absorption capacity of SAPs decreased significantly with increasing crosslinking degrees, where low crosslinked SAPs exhibited the highest adsorption capacity.

Previous studies have established that the water absorption capacity of SAPs is influenced by pH and ionic strength [20]. In this study, the pH and salt resistance of SAPs were enhanced by incorporating isopropylacrylamide into their ionic networks to copolymerize with acrylic acid (Figure S1). The swelling degree of SAPs was indeed affected by both pH and ionic strength (Fig. 1C and D). In general, low crosslinked SAPs exhibited better water absorption compared to those with medium/high crosslinking degrees. To achieve better absorption, using higher concentrations of SAPs is effective. As demonstrated in Figure S2 and S3, taking SAP-0.75 as an example, when 40 mg/mL of SAPs is utilized, the volume of a 300 mM NaCl solution still decreases to 38.83%. Additionally, for solutions with varying pH levels, over 85.67% of the solution is absorbed. These observations suggest that SAPs are efficient at absorbing water molecules, and their absorption capacity can be modulated by adjusting the degree of crosslinking, the incubation time or the concentration of SAPs. Based on these results, low crosslinked SAPs emerged as the most effective for preconcentrating CCM before the isolation of EVs.

To assess whether SAPs affect the level of EVs in CCM during absorption and concentration, MSC-EVs isolated by UC were added to PBS and then incubated with 10 mg/mL SAPs for 180 min. The volume of the EV-containing solution decreased after absorption, resulting in a concentrated EV solution (Figure S4). NTA analysis revealed that initial EV concentration (1×10^9 particles/mL) increased to over 1.1×10^9 particles/mL after absorption with low crosslinked SAPs, indicating a more than 110% increase in EV concentration after a single, simple incubation step (Fig. 1E). This increase is likely due to the small water channel size of the SAPs, which is smaller than the size of MSC-EVs. However, the yield of SAP-0.25 and SAP-0.5 in the low crosslinked group was

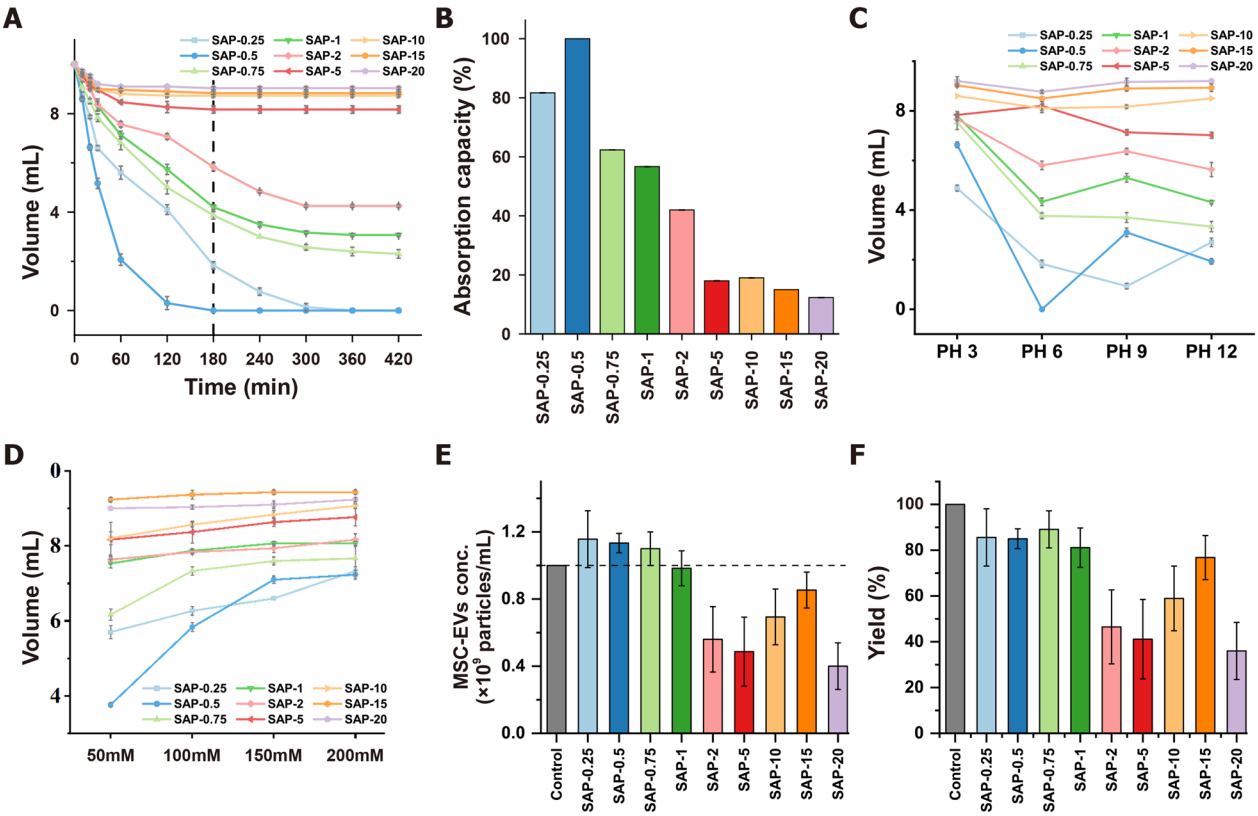

Fig. 1 Characterization of superabsorbent polymers (SAPs) for concentrating extracellular vesicles (EVs) by using ionic network. **A** Water absorption and volume reduction curves of SAPs with different crosslinking degrees over time. **B** Water absorption capacity of different crosslinking degree SAPs. **C** pH-dependent water absorption and volume reduction profiles of SAPs for 180 min; **D** Ionic strength-dependent water absorption and volume reduction profiles of SAPs for 180 min; **E** Concentration capacity of SAPs in mesenchymal stem cell-derived extracellular vesicles (MSC-EVs) standard solution for 180 min. **F** Yield of MSC-EVs concentrated by using SAPs for 180 min

less than 86%, possibly because their water channel size is comparable to the size of MSC-EVs. In contrast, most EVs were retained in the non-absorbed solution of SAP-0.75, achieving a final EV yield of 89% post-concentration (Fig. 1F).

The adsorption capacity of SAP-0.75 for protein impurities in CCM was measured using the BCA assay. The results revealed that even as the volume of CCM decreased, the protein concentration did not increase as it did with MSC-EVs, but rather, significantly decreased (Figure S5A). Surprisingly, considering the volume change of CCM before and after concentration, the absolute amount of protein impurities dramatically reduced from 41.49 μg to 28.73 μg (Figure S5B). This simple incubation process not only increased the concentration of MSC-EVs in the CCM but also removed 30.75% of the protein impurities. We hypothesize that the observed effects are due to the size differences among the water channels of the SAPs, the MSC-EVs, and the protein impurities. Specifically, the impurities, being smaller than the water channels, were extensively adsorbed by the SAP, whereas the larger MSC-EVs were excluded. To substantiate this hypothesis, we tested whether SAP-0.75 could selectively absorb gold nanoparticles of 5 nm, 20 nm, and 100 nm in diameter. SAP-0.75 was incubated with gold nanoparticles of varying sizes for 1 h, after which the SAPs was observed. As shown in the Figure S6, SAP incubated with 5 nm and 20 nm gold nanoparticles displayed wine-red and purple colors, respectively, indicating high levels of gold nanoparticle absorption. In contrast, SAPs incubated with 100 nm gold nanoparticles remained colorless and transparent, similar to SAPs incubated with water, suggesting no absorption of the 100 nm gold nanoparticles. Based on these results, we can infer that the size-dependent adsorption capability of SAPs is responsible for the concentration of MSC-EVs and the removal of protein impurities.

Molecular dynamics simulation

To explore the microstructure and water diffusion behavior, the polymer chain model of SAPs was designed and the fractional free volume (FFV) model

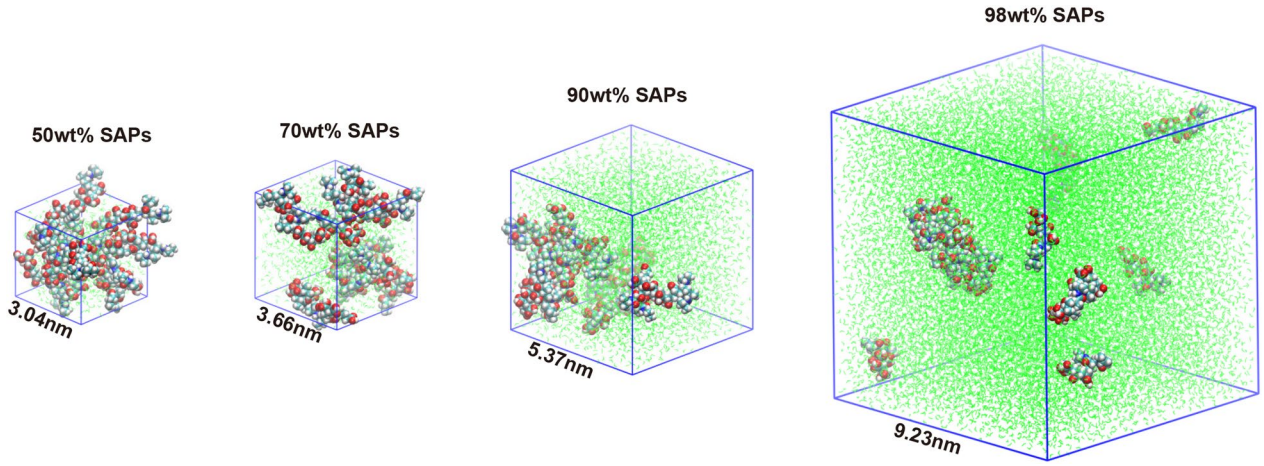

Fig. 2 Molecular dynamics simulation of water absorption in SAPs. Green lines represent water molecules

of the designed polymer chain was simulated the by molecular dynamics [28] (Fig. 2). The behaviour of the FFV with respect to the simulation time is illustrated in Figure S7A. The free volume fraction increases with increasing water content due to the solubilising effect of SAPs on water uptake. The 98% saturated water content model for SAPs has the highest free volume fraction, averaging about 43%.

Utilizing molecular dynamics simulation, the number of hydrogen bonds formed between SAPs and water was quantified, in order to assess the hydration capacity of SAPs (Figure S7B). It was found that the number of hydrogen bonds between SAPs and water increased with the increasing water content. In models containing 50wt% and 70wt% water content, after 5000 ps, the number of hydrogen bonds continued to rise over time. This increase was attributed to the predominantly stable nature of bound water within SAPs. However, at higher water contents of 90wt% or 98wt%, while the initial number of hydrogen bonds remained high, a decreasing trend was observed over the simulation period. This decrease was likely due to the saturation of bound water sites and the emergence of free water molecules, which exhibit weaker binding interactions with SAPs. The interaction energy of the SAPs with water was divided into Lennard–Jones potential (LJ, nonelectrostatic force) and Coulomb potential (electrostatic force) (Figure S7C and S7D). The interaction energy for water of SAPs, was mainly provided by the electrostatic gravitational force of the Coulomb potential. The change of Coulomb potential energy of models with different water contents is consistent with the hydrogen bond over the simulation time. In other words, the hydration ability of SAPs was endowed by the charge effect that facilitates the attraction of water molecules to form more hydrogen bonds with hydrophilic groups.

Charge neutralization of sodium polyacrylate (SP) and isolation of MSC-EVs by the IOSCE

EVs are negatively charged due to their phospholipid bilayer membranes, which allows them to be aggregated and precipitated by charge-based precipitation. In this study, SP was selected to isolate MSC-EVs by charge neutralization. As shown in Figure S8, SP effectively removes water molecules surrounding the EVs, disrupting their hydration layer and increasing their hydrophobicity, which in turn leads to EV aggregation and precipitation [29, 30]. WB analysis revealed that EV markers isolated using 4% SP exhibited higher signal intensity compared to those isolated with other SP concentration (Figure S9). NTA analysis showed that MSC-EVs isolated using 4% SP had an average size of 159.5 ± 64.7 nm, with a narrower distribution range than those obtained with other concentrations, suggesting a more uniform vesicle size distribution within the samples (Figures S10, S11, Table S2). Based on these findings, 4% SP was chosen for subsequent experiments to isolate MSC-EVs in combination with SAPs concentration. Additionally, the 4% SP proved effective in separating EVs from plasma (Figure S12 and S13).

To assess our proposed IOSCE method, CCM harvested from human umbilical cord MSCs was treated with the combination of SAP-0.75 and 4% SP (Fig. 3A). This was compared to UC and PEG-based precipitation methods (20% PEG-6000) (Table S3). The median size of the isolated particles of IOSCE was 176.8 ± 75.4 nm, showing no significant difference compared to the

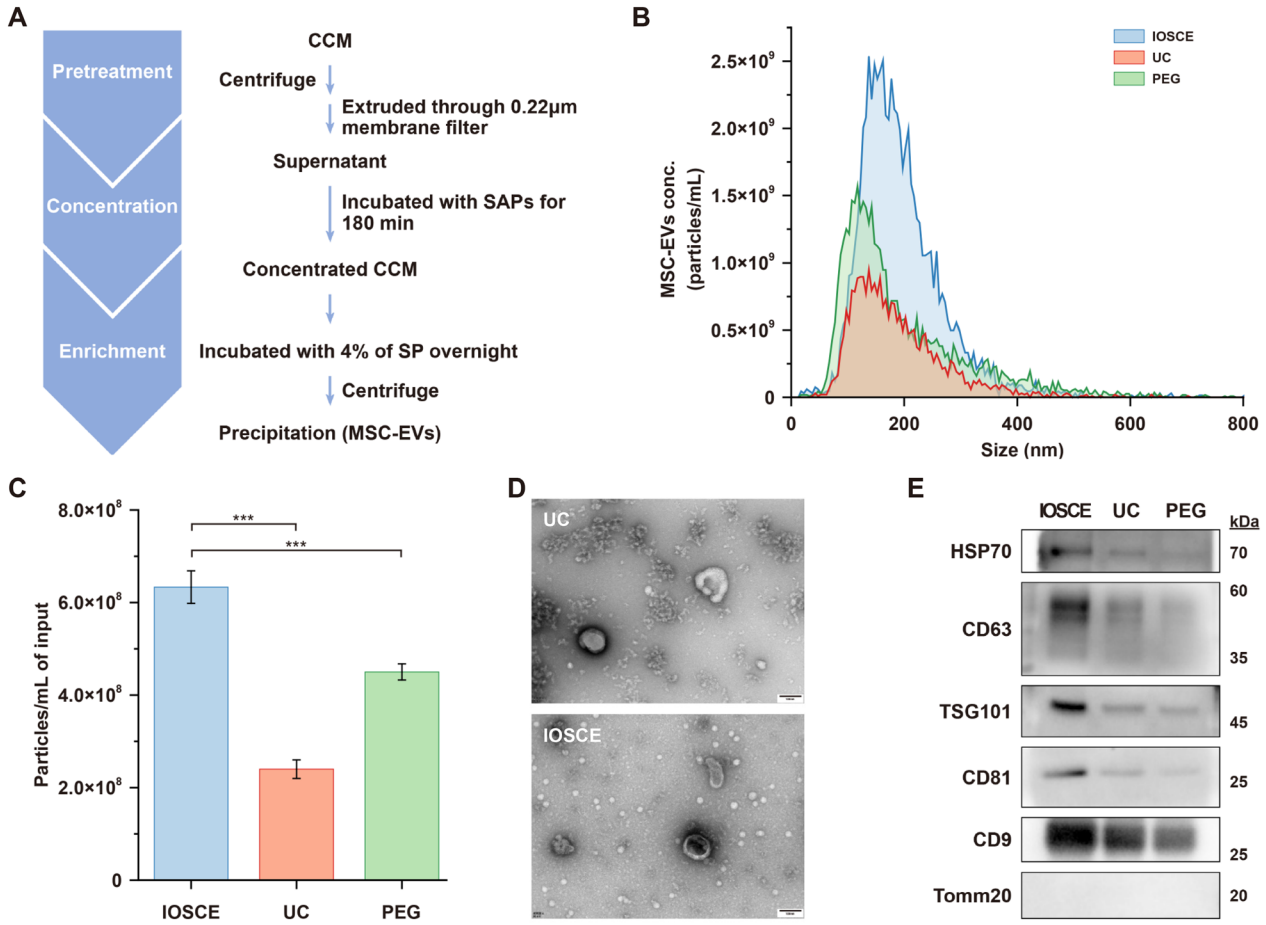

Fig. 3 Isolation of MSC-EVs by using the IOSCE, UC and PEG. **A** Flow chart of MSC-EVs isolation by the IOSCE. **B** Particle size distributions and concentration of MSC-EVs isolated by different methods from CCM. The particle concentrations have been corrected for sample input volumes. **C** Particle yields of each method. Particle yields have been corrected for sample input volumes. **D** TEM images of MSC-EVs obtained by UC and the IOSCE. Scale bars = 100 nm. **E** Western blots of HSP70, CD63, TSG101, CD81, CD9 and Tomm20 for MSC-EVs isolated from CCM by different methods

other two methods (UC = 164.7 ± 81.5 nm; 20% PEG = 154.3 ± 115 nm), all within the size range of small EVs (Fig. 3B). The yields of the MSC-EVs isolated by IOSCE was $(6.33 \pm 0.35) \times 10^8$ particles/mL, which is 2.64 times and 1.4 times higher than those isolated by UC and 20% PEG, respectively (Fig. 3C). Due to the lower centrifugal force, MSC-EVs isolated by IOSCE exhibit a more typical cup-shaped morphology compared to those obtained by UC (Fig. 3D). These findings indicate that the IOSCE, effectively isolates MSC-EVs within the characteristic size range, and achieves a higher yield of MSC-EVs with more intact morphology.

Moreover, the results obtained from WB also proved the same conclusion. EVs were isolated from the same volume of CCM using three different methods, and the protein contents of CD9, CD81, CD63, TSG101, HSP70 and Tomm20 were compared. As shown in Fig. 3E, the protein expression levels of canonical EV markers (CD9, CD81, CD63, TSG101 and HSP70) were significantly higher in the IOSCE methods, indicating that IOSCE can yield more EVs from the same volume of CCM. Furthermore, the absence of the negative marker (Tomm20) signal in EVs indicated the elimination of cellular impurities. To evaluate the purity of MSC-EVs enriched using the IOSCE method, we examined two key indicators: the particle-to-protein ratio and the RNA-to-protein ratio. As shown in Table S4 and S5, the MSC-EVs enriched by IOSCE had a particle-to-protein ratio of $(7.22 \pm 0.4) \times 10^{10}$ particles/μg and an RNA-to-protein ratio of 129.5 ± 10.2 pg/μg. Compared to traditional methods such as ultracentrifugation (UC), size exclusion chromatography (SEC), and polymer precipitation, the IOSCE method achieved superior purity levels.

The IOSCE method was employed to enrich MSC-EVs from 500 mL of CCM in order to assess the scalability of this approach. As shown in Figure S14A and D, the

particle size of EVs enriched from the large sample volume was within the expected nanometer range, with a characteristic cup-shaped morphology, consistent with the standards for small EVs. As depicted in Figure S14B, the MSC-EV yield was $(6.43 \pm 0.12) \times 10^8$/mL. Both particle size distribution and yield were consistent with the results obtained from smaller sample volumes. Moreover, we characterized the typical small EV markers, CD9, TSG101, and CD63, via WB, all of which produced clear bands, and there is no contaminating protein Tomm20, a mitochondrial marker (Figure S14C).

These findings underscore the efficacy and scalability of IOSCE for the maximal concentration of CCM and the efficient isolation of EVs, suggesting that IOSCE is a more effective method than UC and precipitation methods for isolating EVs from CCM.

Evaluation of inhibiting effect of MSC-EVs isolated by the IOSCE on LPS-induced neuroinflammation in microglial cells

In this study, the anti-inflammatory effect of MSC-EVs isolated using the IOSCE was investigated using mouse microglial cell lines (BV2 cells). Prior to this, in vitro cytotoxicity and hemolysis assays were conducted on MSC-EVs obtained via the IOSCE method to assess their safety and biocompatibility. Enriched MSC-EVs were first incubated with BV2 cells, with groups divided based on varying doses, and cell viability was monitored. As shown in Figure S15A, Calcein-AM/EthD-1 double staining revealed strong viability and growth in both the dosing and control groups, with minimal cell death (red fluorescence indicating EthD-1-staining dead cells). Furthermore, CCK-8 assays were employed to assess the effects of MSC-EVs on BV2 cell growth. As shown in the Figure S15B, BV2 cells in the dosing groups exhibited robust viability compared to the NC group, with values of $124.34 \pm 8.06\%$, $120.67 \pm 10.12\%$, $118.02 \pm 13.04\%$, and $97.06 \pm 3.28\%$, respectively. Additionally, the hemolysis assay demonstrated no observable hemolytic activity at MSC-EVs concentrations up to 60 μg/mL (Figure S15C). Taken together, these results indicate that the enriched MSC-EVs exhibit excellent biosafety, providing a solid foundation for downstream applications and the development of clinical therapies.

To establish a neuroinflammation model, LPS-induced BV2 cells were used, as LPS can stimulate the release of inflammatory cytokines in various cell types. The optimal therapeutic concentration of MSC-EVs was first explored. As shown in Figure S16, cell viability gradually increased as the concentration of MSC-EVs rose from 0 μg/mL to 60 μg/mL. The maximum viability was observed at a concentration of 30 μg/mL, after which there was a slight decrease. Therefore, we determined that 30 μg/mL of MSC-EVs as the optimized concentration for subsequent experiments. The MSC-EVs were effectively internalized by the BV2 cells (Fig. 4A). Microglia, as tissue-specific macrophages, share common macrophage characteristics and exist in two distinct activation states: the classical pro-inflammatory M1 state and the anti-inflammatory M2 state [31]. To elucidate the specific effect of LPS on microglial activation, the expression levels of the M1 marker (CD16) and the M2 marker (Arg1) were analyzed

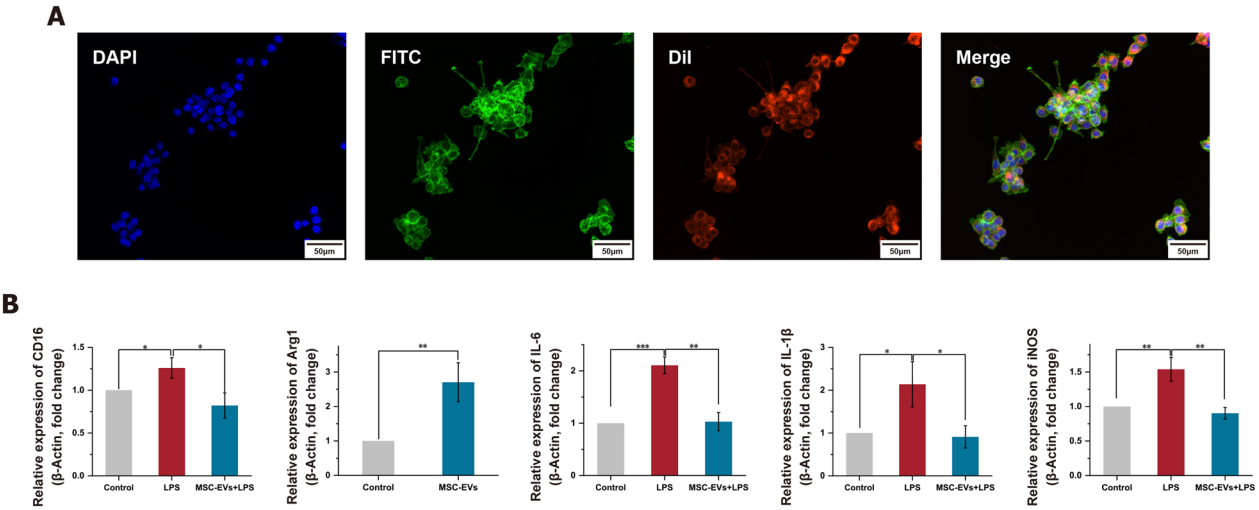

Fig. 4 The effect of MSC-EVs isolated by IOSCE on the lipopolysaccharides (LPS)-induced neuroinflammation. **A** Confocal images of the internalization of DiI-labeled MSC-EVs (red) by BV2 cells. Nucleus and cytoskeleton of the BV2 cells were labeled by 4′,6-diamidino-2-phenylindole (DAPI, blue) and fluorescein isothiocyanate (FITC, green), respectively. Scale bars = 50 μm. **B** mRNA levels of CD16, Arg1, IL-6, IL-1β and iNOS as detected using quantitative real-time PCR. Significant differences are indicated (*$p < 0.05$, **$p < 0.01$, ***$p < 0.001$)

via qRT-PCR (Fig. 4B). The expressions of CD16 were significantly upregulated after LPS treatment, but this upregulation was significantly reduced by pretreatment with MSC-EVs ($p < 0.05$). Conversely, Arg1 expression showed a significant increase with MSC-EVs pretreatment ($p < 0.01$). These results suggest that MSC-EVs can inhibit M1 microglial polarization while promoting M2 polarization. Additionally, the levels of pro-inflammatory factors, IL-6, IL-1β and iNOS, were investigated using qRT-PCR (Fig. 4B). MSC-EVs were found to significantly reduce the release of these pro-inflammatory factors, a finding further corroborated by ELISA results (Figure S17). This comprehensive analysis indicates the potential of MSC-EVs in modulating inflammatory responses in microglial cells.

Proteomic analysis of the effects of MSC-EVs on LPS-induced neuroinflammatory response in BV2 cells

In this study, the effects of MSC-EVs on neuroinflammation were further explored by conducting a high-throughput proteomic analysis. Control, LPS-treated, MSC-EVs-treated and MSC-EVs + LPS-treated BV2 cells were identified by using DIA mass spectrometry. Data independent acquisition (DIA) was chosen for its high data completeness and robust performance (Fig. 5A). A DIA library of about 3025 proteins was computationally merged from untreated and treated samples and a direct-DIA search for all single-run samples. On average, 2863 proteins were at a 1% peptide FDR quantified per sample (Fig. 5B). The data acquired had high completeness, with 100% completeness for 2847 proteins (99.27%), 75% for 2867 proteins (99.93%), and 50% for 2867 proteins (99.97%) (Figure S18). A total of 2847 proteins present in all runs were used in the subsequent analyses. The relative abundance of the quantified proteins (normalized as iFOT) spanned six orders of magnitude after logarithmic transformation, which reflected the deep sequencing coverage (Fig. 5C, Figure S19).

Subsequently, the impact of MSC-EVs on BV2 cells were assessed by differential expression analysis. Remarkably, exhibited no significant change, with only 7 proteins showing significant alterations [FDR < 0.05, Fold change (FC) > 2] (Fig. 6A). Notably, proteins in the NF-κB pathway, crucial in cellular response to stimuli, showed no

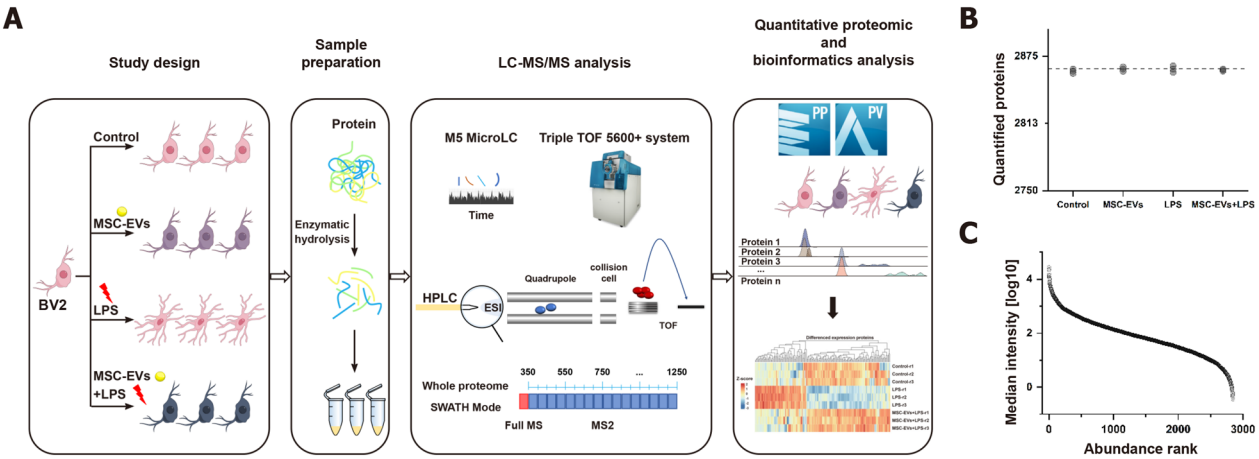

Fig. 5 Study design and proteome characterization of the effects of MSC-EVs on LPS-induced neuroinflammatory response in BV2 Cells. **A** Overview of the study groups and schematic proteomic workflow. **B** Number of proteins identified and quantified passing the 1% false discovery rate (FDR) cutoffs in each sample. The dashed line indicates the mean of the quantified proteins. **C** Median protein abundance distribution of quantified proteins based on iFOT intensities

(See figure on next page.)

Fig. 6 Differential proteomic analysis and bioinformatics analysis of the impact of MSC-EVs on BV2 cells. **A** Volcano plot for quantitative proteins between control and MSC-EVs-treated BV2 cells. The horizontal dashed line shows an FDR of 0.05. The vertical dashed lines show a fold change (FC) of 2. **B** The differentially expressed proteins on control and MSC-EVs-treated BV2 cells (FDR < 0.05). The bigger circle, the greater the differential expression level. Out to inner numbers in circles represented logarithmic values of the fold changes and the expression levels of group control and MSC-EVs-treated BV2 cells. **C** Volcano plot for quantitative proteins between MSC-EVs + LPS-treated and LPS-treated BV2 cells. The horizontal dashed line shows an FDR of 0.05. The vertical dashed lines show an FC of 2. **D** GO enrichment analysis on differentially expressed proteins between MSC-EVs + LPS-treated and LPS-treated BV2 cells. **E** The protein expression levels of six spliceosomal proteins of control, LPS-treated, and MSC-EVs + LPS-treated BV2 cells. **F** The heatmap analysis of differential proteins between LPS vs. control and MSC-EVs + LPS vs. LPS. **G** The Mfuzz analysis of differential proteins between LPS vs. control and MSC-EVs + LPS vs. LPS

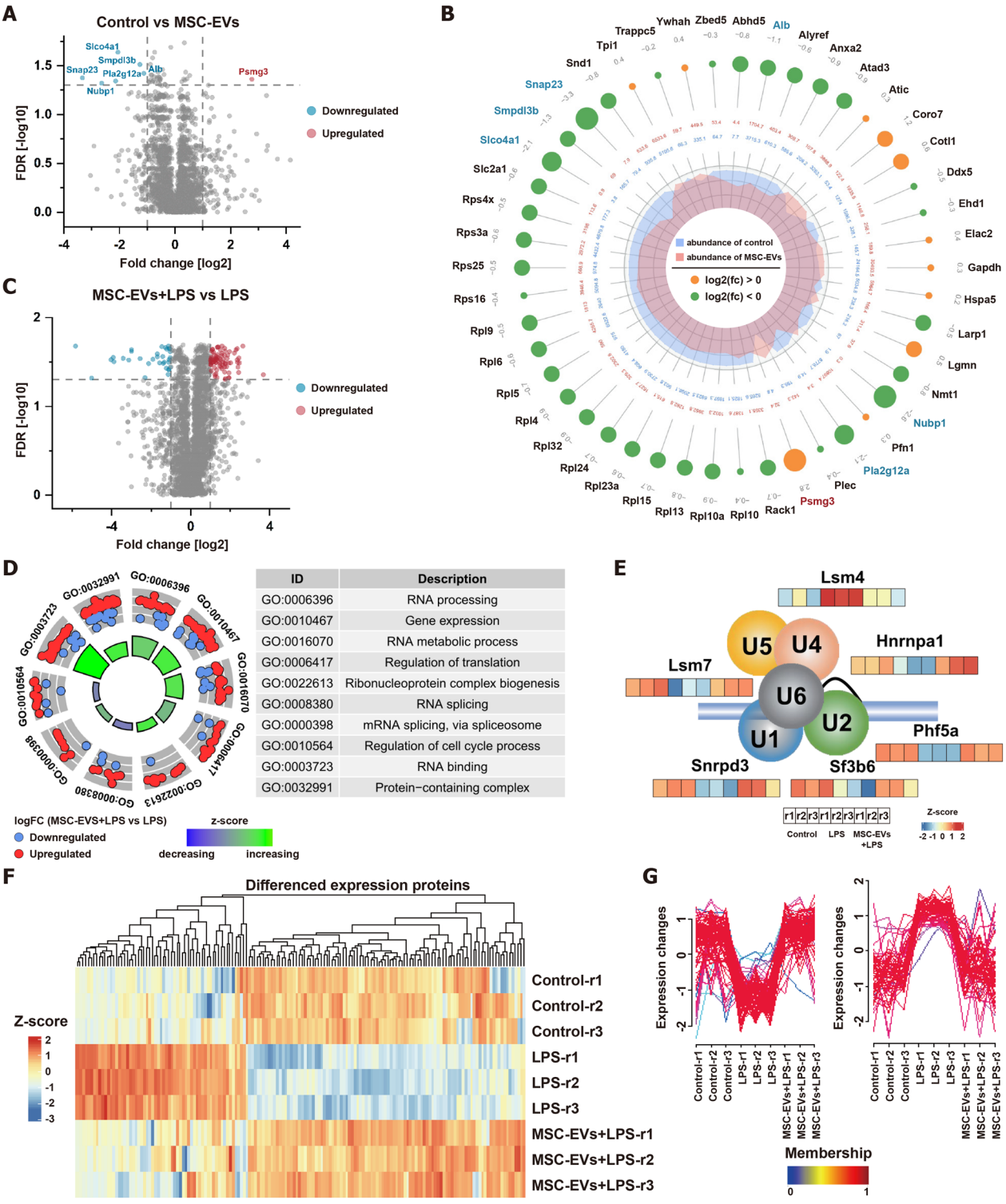

ID	Description
GO:0006396	RNA processing
GO:0010467	Gene expression
GO:0016070	RNA metabolic process
GO:0006417	Regulation of translation
GO:0022613	Ribonucleoprotein complex biogenesis
GO:0008380	RNA splicing
GO:0000398	mRNA splicing, via spliceosome
GO:0010564	Regulation of cell cycle process
GO:0003723	RNA binding
GO:0032991	Protein−containing complex

Fig. 6 (See legend on previous page.)

significant changes. However, the negative regulator of this pathway, smpdl3b, was downregulated (Fig. 6B). The protein Psmg3, known to be downregulated in response to INF-γ and related to inflammatory responses, was significantly upregulated in MSC-EVs internalized by BV2 cells, suggesting a potential anti-inflammatory role. This

aligns with our phenotypic observations of an increase in M2-type BV2 cells, indicating that MSC-EVs minimally affect protein expression in BV2 cells and may promote an anti-inflammatory state.

Further differential protein analysis was conducted to evaluate the effects of LPS on BV2 cells and the anti-inflammatory potential of MSC-EVs. 105 proteins were significantly changed after LPS stimulation (FDR < 0.05, FC > 2) (Figure S20), predominantly related to RNA metabolic processes and regulation of translation (Figure S21). By comparing the protein expression profiles of LPS-stimulated BV2 cells pretreated with and without MSC-EVs, 113 proteins were significantly changed (FDR < 0.05, FC > 2) (Fig. 6C). Interestingly, the expression of functionalized differential proteins was also related to RNA metabolic process and regulation of translation, similar to the biological processes involved in differential proteins in BV2 cells before and after LPS stimulation (Fig. 6D). Notably, MSC-EVs effectively countered significant LPS-induced alterations in RNA metabolism and transcriptional regulatory proteins (Figure S22). For example, MSC-EVs restored normal levels of six spliceosomal proteins involved in RNA splicing (Fig. 6E). A combined analysis of differential proteins between LPS vs. control and MSC-EVs + LPS vs. LPS through heatmap and Mfuzz analyses revealed that MSC-EVs broadly offset LPS-induced protein changes (Fig. 6F and G). Consequently, MSC-EVs appear to restore cells to their baseline state by reversing LPS-induced alterations in biological processes, emphasizing their potential in RNA metabolism and translational regulation modulation.

Conclusions

Over the past few decades, significant progress has been made in the study and translational applications of EVs. However, the gap between the low yield of EVs and the high demand for their application remains inadequately addressed [32–36].

To tackle this issue, we developed an ion osmolarity-driven sequential concentration-enrichment strategy to isolate EVs from umbilical cord mesenchymal stem CCM. We compared the performance of this method with the commonly used UC and PEG precipitation techniques. Our results demonstrate that the EVs isolated using this strategy meet the standard characteristics of EVs [37], such as particle size, morphology, and surface markers. Importantly, the yield was significantly higher than that of UC (2.64 times) and PEG precipitation (1.41 times), and the EVs exhibited excellent biosafety and biological activity. Furthermore, our scalability study confirmed that this method can process 500 mL of CCM without compromising EV characteristics or yield.

As previously mentioned, the sequential concentration-enrichment strategy plays a crucial role in achieving high yield and scalable EV isolation. In fact, current EV isolation methods rarely include a concentration step [38, 39]. However, when dealing with hundreds of milliliters of CCM, pre-concentration without damage is essential to reduce the pressure on downstream enrichment steps. The few studies that report such methods typically employ commercially available SAPs with limited design flexibility [20]. In contrast, we developed a novel SAP composed of N-isopropylacrylamide and N,N′-methylene-bisacrylamide with a crosslinking density of 0.75%, which exhibited 13.62 times the water absorption capacity of commercial SAPs. During the enrichment phase, large-scale EV preparation often relies on ultracentrifugation and ultrafiltration. However, the high centrifugal forces and transmembrane pressure can potentially damage EVs, affecting yield [40, 41]. In this study, we addressed this issue by developing a novel charged polymer to enrich EVs. This polymer utilizes ion osmotic pressure to precipitate EVs and improves enrichment specificity through electrostatic interactions with EV surfaces. It avoids the damaging effects of high centrifugal force, allowing for high-yield, high-purity EVs without compromising their biological activity.

Nonetheless, while the IOSCE strategy has proven successful at the laboratory scale, challenges may arise in large-scale industrial production, such as equipment adaptability, process stability, and controllability. Therefore, detailed quality control steps will need to be established for the large-scale production of EVs.

In summary, we have proposed a sequential concentration-enrichment strategy that effectively isolates biologically active EVs. This strategy utilizes the ionic osmotic pressure to concentrate EVs by trapping water containing hydrophilic groups in the ion network, and neutralize the charge to isolate the EVs. This strategy enables large scale production and high yields of EVs. Moreover, the isolated MSC-EVs have shown the ability to attenuate neuroinflammation, indicating their potential in disease treatment. Overall, this strategy holds promise in the fields of EV isolation and therapeutic applications.

Supplementary Information

The online version contains supplementary material available at https://doi.org/10.1186/s12951-024-02956-w.

Additional file 1. Materials; cell culture; evaluation of the SAPs; molecular dynamics simulation; MSC-EVs isolation by UC and PEG-based precipitation; NTA; TEM; protein abundance quantification and WB; Scaled-up isolation of MSC-EVs by using the IOSCE; The safety and biocompatibility assessments; MSC-EVs internalization; ELISA and qRT-PCR; proteomic sample preparation; LC–MS/MS analysis; data retrieval and quantitative analysis; bioinformatics analysis; synthetic formulations of SAPs; NTA data of MSC-EVs; comparative analysis of IOSCE's performance and methods in references; synthesis schematic of SAPs; effect of salt and PH on water absorption of SAPs; water absorption capacity of SAPs; molecular dynamics simulation of water absorption in SAPs; SP isolation principle; representative markers and NTA of MSC-EVs; NTA data of plasma EVs; WB results of plasma EVs; ELISA results of pro-inflammatory cytokines; data completeness curve; protein abundance distribution of quantified proteins; volcano plot for quantitative proteins; GO enrichment analysis; volcano plot for quantitative proteins.

Acknowledgements
Not applicable.

Author contributions
W.L.: Conceptualization, Methodology, Formal analysis, Writing—Original Draft, Visualization. X.J.: Validation, Data curation. G.X.: Resources, Investigation. S.Y.: Investigation, Data curation. Z.M.: Investigation, Formal analysis. W.F.: Validation, Formal analysis. Z.B.: Formal analysis, Data curation. L.L.: Funding acquisition, Writing—review & editing, Visualization. L.J.: Supervision, Funding acquisition, Writing—review & editing. All of the authors have read and approved the final manuscript.

Funding
This work was supported by the National Natural Science Foundation of China (No. 22004012), DMU-1&DICP (DMU-1&DICP UN202204), the Liaoning Directed Project for Planning of Science and Technology (No. 2021JH2/10300135) and the Dalian High-level Talent Team Project (No. 2022RG18).

Availability of data and materials
No datasets were generated or analysed during the current study.

Declarations

Ethics approval and consent to participate
The use of human umbilical cord mesenchymal stem cells was approved by the Ethics Committee of the First Affiliated Hospital of Dalian Medical University (approval PJ-KS-KY-2023-97). All procedures were in compliance with the relevant guidelines and regulations.

Consent for publication
The authors confirm that the work described has not been published before, not under consideration for publication elsewhere. Its publication has been approved by all co-authors.

Competing interests
The authors declare no competing interests.

Author details
[1]Stem Cell Clinical Research Center, The First Affiliated Hospital of Dalian Medical University, Dalian 116011, China. [2]State Key Laboratory of Medical Proteomics, National Chromatographic R. & A. Center, CAS Key Laboratory of Separation Science for Analytical Chemistry, Dalian Institute of Chemical Physics, Chinese Academy of Sciences, Dalian 116023, China.

Received: 19 August 2024 Accepted: 26 October 2024
Published online: 10 November 2024

References

1. Thakur A, Ke X, Chen YW, Motallebnejad P, Zhang K, Lian Q, Chen HJ. The mini player with diverse functions: extracellular vesicles in cell biology, disease, and therapeutics. Protein Cell. 2022;13(9):631–54.
2. Robbins PD, Morelli AE. Regulation of immune responses by extracellular vesicles. Nat Rev Immunol. 2014;14(3):195–208.
3. Jeppesen DK, Fenix AM, Franklin JL, Higginbotham JN, Zhang Q, Zimmerman LJ, Liebler DC, Ping J, Liu Q, Evans R, Fissell WH, Patton JG, Rome LH, Burnette DT, Coffey RJ. Reassessment of exosome composition. Cell. 2019;177(2):428-445.e18.
4. Pluchino S, Smith JA. Explicating exosomes: reclassifying the rising stars of intercellular communication. Cell. 2019;177(2):225–7.
5. Boriachek K, Masud MK, Palma C, Phan HP, Yamauchi Y, Hossain MSA, Nguyen NT, Salomon C, Shiddiky MJA. Avoiding pre-isolation step in exosome analysis: direct isolation and sensitive detection of exosomes using gold-loaded nanoporous ferric oxide nanozymes. Anal Chem. 2019;91(6):3827–34.
6. Zhang H, Tang Y, Zhou Y, Wang Y, Si H, Li L, Tang B. DNAzyme-RCA-based colorimetric and lateral flow dipstick assays for the point-of-care testing of exosomal m5C-miRNA-21. Chem Sci. 2024;15(24):9345–52.
7. Zhang P, Jiang J, Zhou X, Kolay J, Wang R, Wan Z, Wang S. Label-free imaging and biomarker analysis of exosomes with plasmonic scattering microscopy. Chem Sci. 2022;13(43):12760–8.
8. Gao F, Jiao F, Xia C, Zhao Y, Ying W, Xie Y, Guan X, Tao M, Zhang Y, Qin W, Qian X. A novel strategy for facile serum exosome isolation based on specific interactions between phospholipid bilayers and TiO2. Chem Sci. 2018;10(6):1579–88.
9. Lin Z, Wu Y, Xu Y, Li G, Li Z, Liu T. Mesenchymal stem cell-derived exosomes in cancer therapy resistance: recent advances and therapeutic potential. Mol Cancer. 2022;21(1):179.
10. Ding JY, Chen MJ, Wu LF, Shu GF, Fang SJ, Li ZY, Chu XR, Li XK, Wang ZG, Ji JS. Mesenchymal stem cell-derived extracellular vesicles in skin wound healing: roles, opportunities and challenges. Mil Med Res. 2023;10(1):36.
11. Xu F, Fei Z, Dai H, Xu J, Fan Q, Shen S, Zhang Y, Ma Q, Chu J, Peng F, Zhou F, Liu Z, Wang C. Mesenchymal stem cell-derived extracellular vesicles with high PD-L1 expression for autoimmune diseases treatment. Adv Mater. 2022;34(1): e2106265.
12. Rather HA, Almousa S, Craft S, Deep G. Therapeutic efficacy and promise of stem cell-derived extracellular vesicles in Alzheimer's disease and other aging-related disorders. Ageing Res Rev. 2023;92: 102088.
13. Niu X, Xia Y, Luo L, Chen Y, Yuan J, Zhang J, Zheng X, Li Q, Deng Z, Wang Y. iPSC-sEVs alleviate microglia senescence to protect against ischemic stroke in aged mice. Mater Today Bio. 2023;19: 100600.
14. Garcia-Contreras M, Thakor AS. Human adipose tissue-derived mesenchymal stem cells and their extracellular vesicles modulate lipopolysaccharide activated human microglia. Cell Death Discov. 2021;7(1):98.
15. Gupta D, Zickler AM, El Andaloussi S. Dosing extracellular vesicles. Adv Drug Deliv Rev. 2021;178: 113961.
16. Tian Y, Gong M, Hu Y, Liu H, Zhang W, Zhang M, Hu X, Aubert D, Zhu S, Wu L, Yan X. Quality and efficiency assessment of six extracellular vesicle isolation methods by nano-flow cytometry. J Extracell Vesicles. 2019;9(1):1697028.
17. Zhu L, Sun HT, Wang S, Huang SL, Zheng Y, Wang CQ, Hu BY, Qin W, Zou TT, Fu Y, Shen XT, Zhu WW, Geng Y, Lu L, Jia HL, Qin LX, Dong QZ. Isolation and characterization of exosomes for cancer research. J Hematol Oncol. 2020;13(1):152.
18. Gardiner C, Di Vizio D, Sahoo S, Théry C, Witwer KW, Wauben M, Hill AF. Techniques used for the isolation and characterization of extracellular vesicles: results of a worldwide survey. J Extracell Vesicles. 2016;5:32945.
19. Jia Y, Yu L, Ma T, Xu W, Qian H, Sun Y, Shi H. Small extracellular vesicles isolation and separation: current techniques, pending questions and clinical applications. Theranostics. 2022;12(15):6548–75.
20. Yang HC, Ham YM, Kim JA, Rhee WJ. Single-step equipment-free extracellular vesicle concentration using super absorbent polymer beads. J Extracell Vesicles. 2021;10(4): e12074.
21. Abraham MJ, Murtola T, Schulz R, Páll S, Smith JC, Hess B, Lindahl E. GROMACS: high performance molecular simulations through multi-level parallelism from laptops to supercomputers. SoftwareX. 2015;1–2:19–25.
22. Páll S, Abraham MJ, Kutzner C, Hess B, Lindahl E. Tackling Exascale Software Challenges in Molecular Dynamics Simulations with GROMACS. Lect Notes Comput Sci. 2015.

23. Pronk S, Páll S, Schulz R, Larsson P, Bjelkmar P, Apostolov R, Shirts MR, Smith JC, Kasson PM, van der Spoel D, Hess B, Lindahl E. GROMACS 4.5: a high-throughput and highly parallel open source molecular simulation toolkit. Bioinformatics. 2013;29(7):845–54.
24. Hess B, Kutzner C, van der Spoel D, Lindahl E. GROMACS 4: algorithms for highly efficient, load-balanced, and scalable molecular simulation. J Chem Theory Comput. 2008;4(3):435–47.
25. Van Der Spoel D, Lindahl E, Hess B, Groenhof G, Mark AE, Berendsen HJ. GROMACS: fast, flexible, and free. J Comput Chem. 2005;26(16):1701–18.
26. Lindahl E, Hess B, Van Der Spoel D. GROMACS 3.0: a package for molecular simulation and trajectory analysis. J Mol Model. 2001;7:306–17.
27. Berendsen H, Van Der Spoel D, Van Drunen R. GROMACS: a message-passing parallel molecular dynamics implementation. Comput Phys Commun. 1995;91:43–56.
28. Zhang C, Sui H, Feng G, You M, Shi W, Meng J. Molecular design of hydrophilized polyethersulfone to enhance water/salt selectivity. Macromol. 2023;56:2027–37.
29. Brownlee Z, Lynn KD, Thorpe PE, Schroit AJ. A novel "salting-out" procedure for the isolation of tumor-derived exosomes. J Immunol Methods. 2014;407:120–6.
30. Boriachek K, Islam MN, Möller A, Salomon C, Nguyen NT, Hossain MSA, Yamauchi Y, Shiddiky MJA. Biological functions and current advances in isolation and detection strategies for exosome nanovesicles. Small. 2018;14(6).
31. Yang X, Xu S, Qian Y, Xiao Q. Resveratrol regulates microglia M1/M2 polarization via PGC-1α in conditions of neuroinflammatory injury. Brain Behav Immun. 2017;64:162–72.
32. Visan KS, Wu LY, Voss S, Wuethrich A, Möller A. Status quo of extracellular vesicle isolation and detection methods for clinical utility. Semin Cancer Biol. 2023;88:157–71.
33. Yang D, Zhang W, Zhang H, Zhang F, Chen L, Ma L, Larcher LM, Chen S, Liu N, Zhao Q, Tran PHL, Chen C, Veedu RN, Wang T. Progress, opportunity, and perspective on exosome isolation—efforts for efficient exosome-based theranostics. Theranostics. 2020;10:3684–707.
34. He C, Zheng S, Luo Y, Wang B. Exosome theranostics: biology and translational medicine. Theranostics. 2018;8:237–55.
35. Shirejini SZ, Inci F. The Yin and Yang of exosome isolation methods: conventional practice, microfluidics, and commercial kits. Biotechnol Adv. 2022;54: 107814.
36. Ding L, Yang X, Gao Z, Effah CY, Zhang X, Wu Y, Qu L. A holistic review of the state-of-the-art microfluidics for exosome separation: an overview of the current status, existing obstacles, and future outlook. Small. 2021;17: e2007174.
37. Welsh JA, Goberdhan DCI, O'Driscoll L, Buzas EI, Blenkiron C, Bussolati B, Cai H, Di Vizio D, Driedonks TAP, Erdbrügger U, Falcon-Perez JM, Fu QL, Hill AF, Lenassi M, Lim SK, Mahoney MG, Mohanty S, Möller A, Nieuwland R, Ochiya T, Sahoo S, Torrecilhas AC, Zheng L, Zijlstra A, Abuelreich S, Bagabas R, Bergese P, Bridges EM, Brucale M, Burger D, Carney RP, Cocucci E, Crescitelli R, Hanser E, Harris AL, Haughey NJ, Hendrix A, Ivanov AR, Jovanovic-Talisman T, Kruh-Garcia NA, Ku'ulei-Lyn Faustino V, Kyburz D, Lässer C, Lennon KM, Lötvall J, Maddox AL, Martens-Uzunova ES, Mizenko RR, Newman LA, Ridolfi A, Rohde E, Rojalin T, Rowland A, Saftics A, Sandau US, Saugstad JA, Shekari F, Swift S, Ter-Ovanesyan D, Tosar JP, Useckaite Z, Valle F, Varga Z, van der Pol E, van Herwijnen MJC, Wauben MHM, Wehman AM, Williams S, Zendrini A, Zimmerman AJ, Théry C, Witwer KW. Minimal information for studies of extracellular vesicles (MISEV2023): From basic to advanced approaches. J Extracell Vesicles. 2024;13(2):e12404.
38. Gupta S, Rawat S, Arora V, Kottarath SK, Dinda AK, Vaishnav PK, Nayak B, Mohanty S. An improvised one-step sucrose cushion ultracentrifugation method for exosome isolation from culture supernatants of mesenchymal stem cells. Stem Cell Res Ther. 2018;9:180.
39. Dong L, Zieren RC, Horie K, Kim CJ, Mallick E, Jing Y, Feng M, Kuczler MD, Green J, Amend SR, Witwer KW, de Reijke TM, Cho YK, Pienta KJ, Xue W. Comprehensive evaluation of methods for small extracellular vesicles separation from human plasma, urine and cell culture medium. J Extracell Vesicles. 2020;10: e12044.
40. Xu R, Greening DW, Zhu HJ, Takahashi N, Simpson RJ. Extracellular vesicle isolation and characterization: toward clinical application. J Clin Invest. 2016;126:1152–62.
41. Li P, Kaslan M, Lee SH, Yao J, Gao Z. Progress in exosome isolation techniques. Theranostics. 2017;7:789–804.

Publisher's Note